Nano Research 2015, 8(4): 1081–1097
DOI 10.1007/s12274-014-0586-9
Research Article
ISSN 1998-0124
CN 11-5974/O4

Understanding the stability and reactivity of ultrathin tellurium nanowires in solution: An emerging platform for chemical transformation and material design

Liang Xu, Hai-Wei Liang, Hui-Hui Li, Kai Wang, Yuan Yang, Lu-Ting Song, Xu Wang, and Shu-Hong Yu (✉)

Division of Nanomaterials and Chemistry, Hefei National Laboratory for Physical Sciences at Microscale, Collaborative Innovation Center of Suzhou Nano Science and Technology, Department of Chemistry, University of Science and Technology of China, Hefei 230026, China

Received: 28 July 2014
Revised: 11 September 2014
Accepted: 16 September 2014

KEYWORDS

stability,
reactivity,
oxidation,
reaction kinetics,
chemical transformation,
storage,
ultrathin nanowires

ABSTRACT

The stability and reactivity of nanomaterials are of crucial importance for their application, but the long-term effects of stability and reactivity of nanomaterials under practical conditions are still not well understood. In this study, we first established a comprehensive strategy to investigate the stability of a highly reactive nanomaterial from the viewpoint of reaction kinetics with ultrathin tellurium nanowires (TeNWs) as a model material in aqueous solution through an accelerated oxidation process. This allowed us to propose a new approach for the design and synthesis of other unique one-dimensional nanostructures by a chemical transformation process using the intermediate nanostructures "captured" during the dynamic oxidation process under different conditions. In essence, the oxidation of ultrathin TeNWs is a gas–solid reaction which involves liquid, gas and solid phases. It has been demonstrated that the oxidation process of ultrathin TeNWs in aqueous solution can be divided into three stages, namely oxygen limiting, ultrathin TeNWs limiting and mass transfer resistance limiting stages. The apparent oxidation kinetics for ultrathin TeNWs is approximately in accord with a first order reaction kinetics model and has an apparent activation energy as low as 13.53 kJ·mol^{-1}, indicating that ultrathin TeNWs are thermodynamically unstable. However, the unstable nature of ultrathin TeNWs is actually an advantage since it can act as an excellent platform to help us synthesize and design one-dimensional functional nanomaterials—with special structures and distinctive properties—which are difficult to obtain by a direct synthesis method.

Address correspondence to shyu@ustc.edu.cn

1 Introduction

As a bridge between microcosmic atoms and macroscopic materials, nanomaterials have received considerable attention in recent years [1–11]. However, the long-term effects of stability and reactivity of nanomaterials under practical conditions are still not well understood [12]. Almost all nanomaterials are far away from equilibrium state [13], and generally need a stabilizing environment (such as coating with surfactants or loading on a support) to prevent aggregation between particles and, at the same time, maintain high reactivity during storage and practical applications. Many nanomaterials undergo a dramatic change during practical applications due to a poor stabilizing environment, as has been reported for CdTe nanoparticles [14, 15], CdSe nanoparticles [16], PbSe nanocrystals [17], Ag nanocubes [18], and Cu nanoparticles [19]. Hence, an understanding of the stability and reactivity of nanomaterials, especially in solution, has great value and significance in terms of achieving good performance in actual applications, and also will be helpful in the rational design and synthesis of new nanomaterials. Unfortunately, the relevant data are extremely limited and are usually just derived from some rough and qualitative studies by transmission electron microscopy (TEM) and scanning electron microscopy (SEM). Accordingly, it has become very urgent to establish a reasonable and reliable method to obtain in-depth and comprehensive information about the long-term effects of stability and reactivity of nanomaterials from the viewpoint of reaction kinetics. The goal of a kinetics experiment is to determine the variation in the concentration of one of the reactants or products as a function of time [20]. Compared with other traditional quantitative methods, the absorption spectroscopy method is regarded as the most convenient and practical way to determine the concentration of colloidal nanomaterials, since it does not require tedious, precise, and difficult purification processes [21]. Due to their strongly size-dependent optical properties, the concentration and size of nanomaterials at a certain reaction time have a close relationship with the absorbance and the peak position in the absorption spectrum, which is not the case for traditional polyatomic organic molecules and metal complexes which have constant absorption peaks. Actually, many efforts have already been devoted to explore the growth processes and the growth kinetics of nanomaterials by using the size-dependent optical properties of nanomaterials [22–25].

Ultrathin tellurium nanowires (TeNWs) with diameters of 4–9 nm were first reported in 2006 by our group [26]. Owing to their high reactivity, easy processability, and large-scale synthesis [27], ultrathin TeNWs can be used as an efficient physical or chemical template to generate an extended functional nanomaterial family—including Pt, Pd, Au, Bi_2Te_3, CdTe, PbTe, Ag_2Te, carbonaceous nanofibers and composites—exhibiting extensive applications in many fields, such as catalysis [28–30], supercapacitors [31], thermoelectricity [32], photoconductivity [33] and environmental remediation [34, 35]. Although the high reactivity of ultrathin TeNWs can provide fruitful grounds for exploring new nanoscale structural transformations as well as functionalities of the corresponding templated products, it also gives ultrathin TeNWs a metastable nature, and they can be easily degraded by oxidation during use. Our group have analyzed the structure and morphology evolution of ultrathin TeNWs in different solvents using TEM and SEM observations [36, 37], but quantitative descriptions of these processes are strongly desired.

Herein, we choose ultrathin TeNWs as a model material to study the stability of nanomaterials in aqueous solution from the viewpoint of reaction kinetics and then develop a new approach to material design using their oxidation process as a good platform for chemical transformation. An accelerated oxidation experiment for ultrathin TeNWs was performed in a self-made apparatus (Scheme 1) under different reaction conditions. The chemical kinetics information about this oxidation process was easily obtained by converting ultraviolet–visible (UV–Vis) absorption spectroscopy data. The results indicated that the oxidation kinetics for ultrathin TeNWs was in accord with the first order reaction kinetics model, and the corresponding apparent activation energy was about 13.53 $kJ \cdot mol^{-1}$. Interestingly, after incomplete oxidation, ultrathin TeNWs evolved into a chain-dotted line nanostructure, which still maintained high reactivity and could act as an excellent platform for the

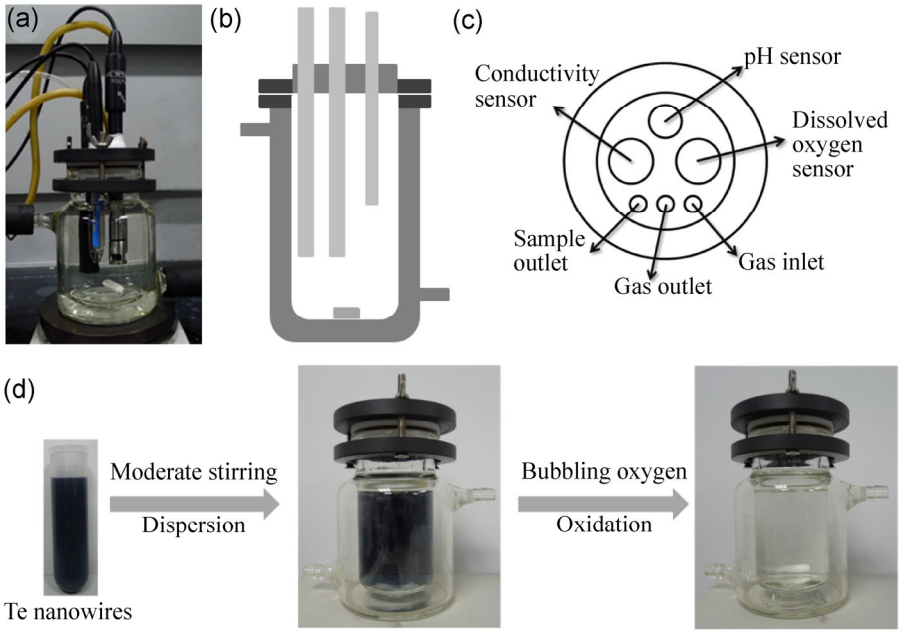

Scheme 1 (a) Photograph of the experimental apparatus for the oxidation kinetics study of ultrathin TeNWs. (b) Schematic diagram of the jacketed pilot plant reactor. (c) Top view of the jacketed pilot plant reactor. (d) The accelerated oxidation experiment for ultrathin TeNWs.

template synthesis of other functional nanomaterials. In addition, we found that oxygen-free conditions and adding suitable reductants can effectively preserve ultrathin TeNWs with uniform morphology and high reactivity during storage.

2 Experimental

2.1 Materials

Na_2TeO_3, poly(vinyl pyrrolidone) (PVP, $M_w \approx 4{,}000$), hydrazine hydrate (85 wt.%), aqueous ammonia solution (25 wt.%–28 wt.%), NaOH, HCl (36%–38%), ethylene glycol (EG), ethanol and H_2PtCl_6 were purchased from Shanghai Chemical Reagents Co. Ltd.. All the chemical reagents were used as received without further purification.

2.2 Synthesis of ultrathin TeNWs

Ultrathin TeNWs with diameters of 4–9 nm were prepared according to the method previously developed by our group [26]. In a typical procedure, 0.0922 g of Na_2TeO_3, 1.0000 g of PVP, 1.65 mL of hydrazine hydrate (85 wt.%) and 3.35 mL of aqueous ammonia solution (25 wt.%–28 wt.%) were added to 32 mL of deionized water with suitable magnetic stirring. The clear mixture was transferred into a 50 mL Teflon-lined stainless steel autoclave. The autoclave was maintained at 180 ℃ for 3 h and then cooled to the room temperature rapidly with cold tap water. The final products were precipitated by adding 150 mL of acetone into the final solution. The precipitates were centrifuged and washed several times with absolute ethanol and distilled water.

2.3 Oxidation of ultrathin TeNWs under different experimental conditions

Firstly, 3 mL of ultrathin TeNWs solution was precipitated by adding 15 mL of acetone. Then the precipitates were collected by centrifuging at 5,000 rpm for 3 min and washed several times with absolute ethanol and deionized water. After that, the precipitates were rapidly dispersed in 35 mL of N_2-staturated deionized water by using a vortex mixer, and the suspension then added to 185 mL of N_2-staturated deionized water with moderate magnetic stirring under the protection of nitrogen, resulting in the formation of a homogeneous suspension. The final concentration of ultrathin TeNWs was about 0.137 mmol/L. The pH of the suspension was carefully

adjusted to the required pH with 1 M NaOH and 1 M HCl. Then oxygen was bubbled into the reaction system with different flow rates, and the suspension was examined by different characterization methods after different time intervals. The temperature of the reaction system was controlled by a precise low temperature thermostat during the experiments.

2.4 Synthesis of Te@C nanocables

The Te@C nanocables were prepared by a template-directed hydrothermal carbonization procedure developed by our group [38, 39]. Briefly, 30 mL of acetone was added into 10 mL of the prepared Te nanowires solution to precipitate the product before centrifuging at 6,000 rpm. The solid was then dispersed into 80 mL of glucose solution (5 g of glucose) with vigorous magnetic stirring for 15 min. Hydrothermal treatment of the mixed solution at 160 ℃ for 24 h resulted in highly uniform Te@C nanocables. The Te@C nanocables were centrifuged and washed several times with absolute ethanol and distilled water.

2.5 Synthesis of Ag_2Te nanowires

After centrifuging and washing, a certain amount of ultrathin TeNWs were redispersed in EG. Then 0.1000 g of silver nitrate was added into the EG suspension of ultrathin TeNWs under vigorous stirring at room temperature, and the color of the suspension changed from blue to brown, suggesting the formation of Ag_2Te nanowires [40]. The Ag_2Te nanowires were centrifuged and washed several times with absolute ethanol and distilled water.

2.6 Synthesis of Pt nanowires

In a typical synthesis, 5 mL of the TeNWs reaction solution was taken out from the reaction system after different oxidation intervals and was degassed by bubbling nitrogen for 15 min. Then, 20 mL of EG and 1.29 mL of 77 mM H_2PtCl_6 solution were added to the solution. The mixture was shaken at a rotation rate of 260 rpm using an Innova 40 Benchtop Incubator Shaker for 20 h at 50 ℃. The products were collected by centrifugation (10,000 rpm, 15 min) and then washed several times with double-distilled water and absolute ethanol.

2.7 Storage of ultrathin TeNWs

A quantity of TeNWs precipitate was redispersed in 10 mL of deionized H_2O to form a homogeneous suspension with vigorous magnetic stirring. Then the suspension was examined at different time intervals during storage. Other experimental samples were prepared by the same procedure with the addition of 1.0000 g PVP, 17.5 mmol of reductants citric acid, ascorbic acid, hydrazine hydrate or aqueous ammonia solution (1 mL), respectively.

2.8 Materials characterization

X-ray powder diffraction (XRD) patterns were obtained from a Philips X'Pert PRO SUPER X-ray diffractometer equipped with graphite-monochromatized Cu Kα radiation (λ = 1.54178 Å). TEM and high-resolution transmission electron microscopy (HRTEM) observations were performed on a JEOL-2010 microscope operated at an acceleration voltage of 200 kV. UV–Vis spectra were recorded on a UV-2501PC/2550 spectrometer (Shimadzu Corp., Japan) at room temperature. The real-time measurements of pH and dissolved oxygen during the experiment were carried out by a digital precision meter (Multi 9430, WTW GmbH., Germany). Inductively coupled plasma atomic emission spectrometry (ICP–AES) measurements were conducted using an AtomScan Advantage spectrometer (Thermo Jarrell Ash Corporation, USA).

3 Results and discussion

3.1 Morphology evolution of ultrathin TeNWs during oxidation

An accelerated oxidation experiment for ultrathin TeNWs was performed in a self-made apparatus (Scheme 1) under different reaction conditions. In our previous study, we found that ultrathin TeNWs were easily oxidized to tellurium dioxide (TeO_2) during storage [36]. Figure 1 shows the morphology evolution of ultrathin TeNWs during an accelerated oxidation process with an oxygen flow rate of 10 sccm. In the initial stage, due to the low dissolved oxygen concentration, the rate of oxidation was very slow and few oxidation etching pits were found on the surfaces of ultrathin TeNWs, which retained good

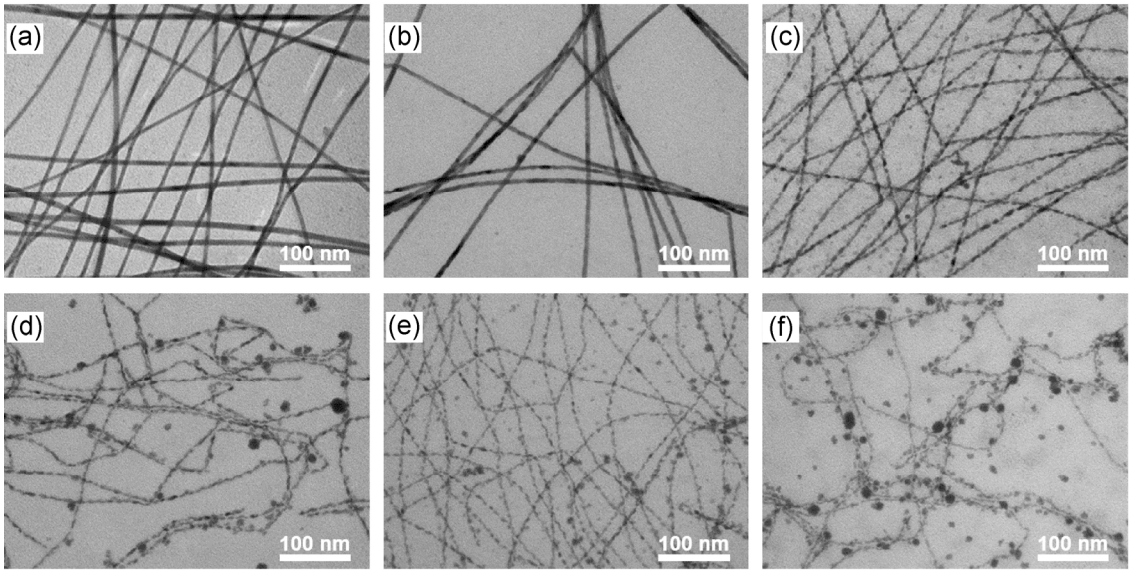

Figure 1 TEM images of morphology evolution of ultrathin TeNWs in water at pH 9 at 298 K with moderate stirring after bubbling oxygen with a flow rate of 10 sccm for: (a) 0; (b) 1; (c) 2; (d) 3; (e) 4; (f) 5 h. Sccm stands for standard cubic centimeters per minute.

one-dimensional nanostructures with smooth surfaces (Figs. 1(a) and 1(b)). With adding oxygen into the reaction system continuously, ultrathin TeNWs were gradually eroded or fractured because of oxidation, and finally formed a special chain-dotted line structure (Figs. 1(c)–1(f)). After oxidation for a long time, the surfaces of ultrathin TeNWs became fairly rough, but they still retained a one-dimensional nanostructure, although it looked as if it was broken in places (Figs. 1(e) and 1(f)) and some oxidation products were attached to form an incomplete oxide shell (Fig. S1 in the Electronic Supplementary Material (ESM)), which blocked further contact between the ultrathin TeNWs and oxygen. In addition, some of the oxidation product TeO_2 were dislodged into the solution from the surfaces of the ultrathin TeNWs and formed uniform nanoparticles with a diameter of about 40 nm (Figs. 1(d)–1(f) and Fig. S2, (in the ESM)). The XRD patterns and HRTEM images and EDS spectra of ultrathin TeNWs during oxidation are shown in Fig. S3 (in the ESM).

3.2 UV–Visible spectra of ultrathin TeNWs and the modified Beer–Lambert law

Ultrathin TeNWs are a p-type semiconductor and their UV–Vis spectrum possesses two broad absorption bands located at about 278 nm (peak I) and 550–650 nm (peak II) [26, 41], which are due to an allowed direct transition (3–6 eV) and a forbidden transition (0–3 eV), respectively [37, 42]. Unlike the case for traditional polyatomic organic molecules and metal complexes, the position of the UV–Vis absorption peak I for ultrathin TeNWs displays a diameter dependence, whereas the position of peak II depends on the length of the ultrathin TeNWs [41, 43]. In Fig. 2(a), we present the evolution of the UV–Vis absorption spectrum of ultrathin TeNWs during oxidation with oxygen at a flow rate of 10 sccm. Other UV–Vis absorption spectra of ultrathin TeNWs under different experimental conditions are given in Figs. S4–S6 (in the ESM). The absorbance intensity of the UV–Vis spectrum decreased as the oxidation process proceeded, suggesting that the concentration of ultrathin TeNWs decreased in solution. The absorption peak I (at 278 nm) decreased gradually during oxidation without any apparent red-shift or blue-shift. This suggests that there was a negligible changes in the diameter of the ultrathin TeNWs during oxidation (since they are already very thin). In contrast, the intensity of the absorption peak II (at 550–650 nm) decreased rapidly on prolonging the reaction time and the peak underwent a significant blue-shift from

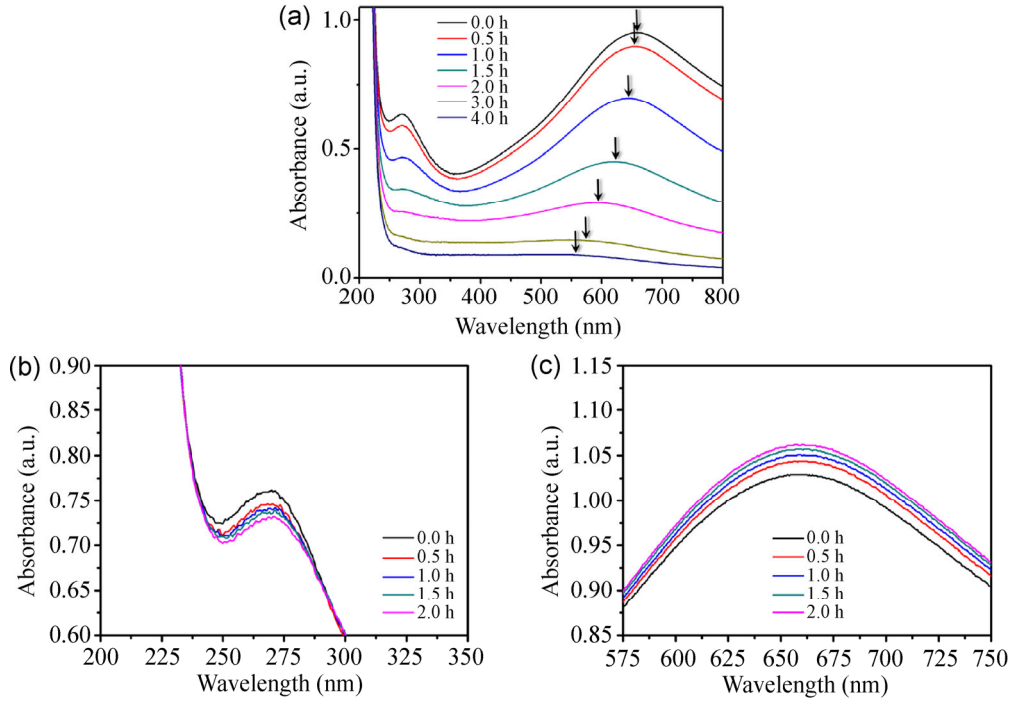

Figure 2 Evolution of UV–Vis absorption spectra for ultrathin TeNWs at pH 9 at 298 K: (a) during oxidation with an oxygen flow rate of 10 sccm; in the range (b) 200–350 nm and (c) 575–750 nm during stirring under the protection of nitrogen.

650 to 550 nm. The blue-shift suggested that the average length of ultrathin TeNWs was decreased [41], which demonstrated that some ultrathin TeNWs were etched and fractured by oxidation (Figs. 1(c)–1(f)). Compared with the absorption peak I (at 278 nm), the absorption peak II (at 550–650 nm) is better able to reflect the changes in ultrathin TeNWs, both in concentration and size, during oxidation.

Owing to the tiny size and flexible features of ultrathin TeNWs, their bundling and intertwining in solution are inevitable, and this can interfere with the absorbance measurements for ultrathin TeNWs. The effects of these factors on the absorbance is manifested in two main ways: (i) scattering of the incident light caused by the aggregation and (ii) shielding of some ultrathin TeNWs from irradiation caused by the cladding. In order to diminish the influence of these effects, it is essential to completely disperse the ultrathin TeNWs into solution. In this study, a moderate magnetic stirring for an extended period was used to form a homogeneous solution of ultrathin TeNWs and reduce bundling and intertwining. The absorbance gradually became stable after moderate magnetic stirring for two hours under the protection of nitrogen (Figs. 2(b) and 2(c)), which demonstrates that appropriate stirring improves the dispersity of ultrathin TeNWs and the accuracy of absorbance measurements. It should be noted that nanoparticles of the oxidized products can also cause light scattering. The scattering intensity of small solids in solution is generally proportional to $1/\lambda^4$ for solid particles which are much smaller than the incident wavelength [44], such as TeO_2 with a diameter about 40 nm; however it is weakly dependent on wavelength for larger particles, such as ultrathin TeNWs with a length more than tens of micrometers. So the use of larger incident wavelength to measure absorption, such as peak II (located at 550–650 nm), allows the effect of light scattering to be reduced as much as possible.

Based on the reasons mentioned above, the typical absorption peak II (located at 550–650 nm) was chosen as a basis for quantitative analysis of UV–Vis absorption of ultrathin TeNWs during oxidation. It is obvious that the absorbance of ultrathin TeNWs is closely related to several factors: concentration, size, dispersity of ultrathin TeNWs and light scattering

caused by ultrathin TeNWs and oxidation products. The impact of dispersity and light scattering on absorbance can be reduced as much as possible through the methods discussed above. In view of the strongly size-dependent optical properties of ultrathin TeNWs, we introduced a correction factor into the Beer–Lambert law to discuss the absorbance of ultrathin TeNWs. Assuming ultrathin TeNWs have an average length of L_i at the time i, the modified Beer–Lambert law can be expressed as follows

$$A_i = \log\frac{I}{I_0} = \varphi_i \cdot \varepsilon l c_i \quad (1)$$

In Eq. (1), A_i is the absorbance of the reaction solution at reaction time i, and c_i is the concentration of ultrathin TeNWs with an average length of L_i, l is the path length, and ε is the extinction coefficient of normal ultrathin TeNWs. The correction factor φ_i was used to adjust the effect of the size of the ultrathin TeNWs on the absorbance, because the extinction coefficient is size-dependent for nanomaterials [45, 46]. Therefore, the traditional method for polyatomic organic molecules and metal complexes, which establishes a working equation by means of a linear regression method, cannot realistically be employed in the case of ultrathin TeNWs. In order to better compare the variation in concentration and size of ultrathin TeNWs under different experiment conditions and decrease the impact of systematic errors under the same conditions, the absorbance data were normalized using the following formula

$$\eta = \frac{A_i}{A_0} = \frac{\varphi_i \cdot \varepsilon l c_i}{\varepsilon l c_0} = \varphi_i \cdot \frac{c_i}{c_0} \quad (2)$$

In Eq. (2), A_0 is the absorbance of the reaction solution before bubbling oxygen, and c_0 is the initial concentration of normal ultrathin TeNWs with an average length of L_0. The normalized variable η consists of two parts: a concentration term c_i/c_0, which represents the fraction of the remaining ultrathin TeNWs in solution, and a correction term φ_i, which compensates for the influence of size evolution. Consequently, the normalized variable η is an objective characteristic of the oxidation process of ultrathin TeNWs from two aspects—both concentration variation and size evolution—and it corresponds to a modified remaining ratio (MRR) for ultrathin TeNWs during oxidation.

3.3 Analysis of the normalized absorption data for ultrathin TeNWs during oxidation

In order to gain in-depth and comprehensive information about the oxidation process, plots of MRR·η versus reaction time (t), and the corresponding differential curves, for different oxygen flow rates are shown in Fig. 3(a) and Fig. S7 (in the ESM). Due to its higher smoothness and better linearity of fit, the curve for an oxygen flow rate of 5 sccm is chosen to discuss the oxidation of ultrathin TeNWs. As the oxidation progressed, the value of MRR·η gradually decreased from 1.0 to approximately zero, which

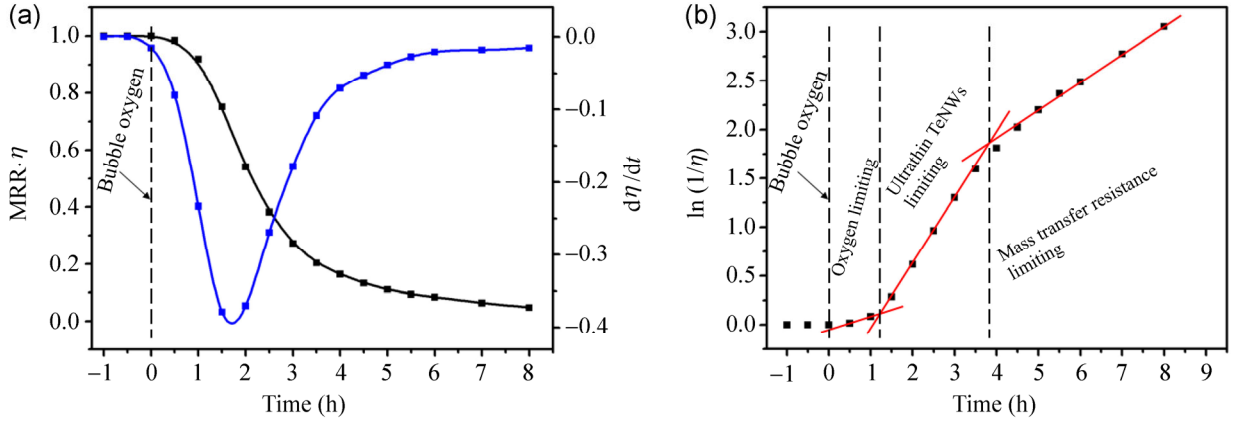

Figure 3 (a) Plot (black) and the corresponding differential curve (blue) of MRR·η versus reaction time t during oxidation with an oxygen flow rate of 5 sccm. (b) Plot of the natural logarithm of the reciprocal of MRR [ln(1/η)] versus reaction time t with an oxygen flow rate of 5 sccm. MRR stands for modified remaining ratio.

reflects the decreases in both concentration and length of the ultrathin TeNWs during oxidation. The corresponding differential curve reveals the rate of change of MRR·η with reaction time. After bubbling oxygen, the differential curve showed a significant minimum at about 1.5 h, which indicated that the rate of concentration decrease of ultrathin TeNWs reached a maximum at this moment.

A plot of the natural logarithm of the reciprocal of MRR [ln(1/η)] versus reaction time (t) was drawn (Fig. 3(b)) to obtain better insight into the reaction mechanism of this oxidation process. Figure 3(b) makes is based on Eq. (3), which is in turn derived from Eq. (2).

$$\ln\frac{1}{\eta} = \ln\frac{c_0}{c_i} + \ln\frac{1}{\varphi_i} \tag{3}$$

According to the different gradients of the plot in different regions, the oxidation process for ultrathin TeNWs can be divided into three stages: oxygen limiting, ultrathin TeNWs limiting and mass transfer resistance limiting. (i) Oxygen limiting occurs in the initial stage when, because of the low dissolved oxygen concentration in solution, the reaction rate is mainly limited by the concentration of dissolved oxygen; (ii) ultrathin TeNWs limiting occurs at longer reaction times, when the concentration of dissolved oxygen has increased (the inset in Fig. 4(a) shows that the concentration of dissolved oxygen (200%, 6.25×10^{-4} M) is almost 4.6 times of the initial concentration of ultrathin TeNWs (1.37×10^{-4} M) after bubbling oxygen for about 0.5 h). In this case, the process starts to become increasingly limited by the concentration of ultrathin TeNWs. When the solution is saturated with oxygen, the effect of oxygen limiting is further weakened, and the reaction rate becomes mainly limited by the concentration of ultrathin TeNWs; (iii) mass transfer resistance limiting arises since due to the solid nature of ultrathin TeNWs, the oxidation products are easily coated on the surfaces of ultrathin TeNWs, which restrains the mass transfer between ultrathin TeNWs and oxygen. When the quantity of oxidation products accumulated to a certain degree, the mass transfer resistance can effectively limit the oxidation of ultrathin TeNWs .

3.4 Reaction kinetics analysis of ultrathin TeNWs oxidation process

The rate of the oxidation process depends strongly on the experimental condition and the downward trend in MRR·η became quicker at high oxygen flow rates, pH values and reaction temperatures (Figs. 4(a), 4(c) and 4(e)). Based on the above, the linear region from 1.5 h to 4.0 h of the plot of [ln(1/η)] versus reaction time (t) (i.e. ultrathin TeNWs limiting) was chosen as a basis to discuss the reaction kinetics of ultrathin TeNWs during oxidation. Figures 4(b), 4(d) and 4(f) show the linear fitting plots of the oxidation process in the range from 1.5 to 4.0 h under different experimental conditions. Equation (4) is the form of the linear fitting equation of these plots. Equations (3) and (4) are equivalent and consist of two terms: a concentration term ln(c_0/c_i) and a correction term ln(1/φ_i) for Eq. (3); variables term (kt) and constant term (q) for Eq. (4). Because the oxidation process of ultrathin TeNWs is mainly affected by the concentration of ultrathin TeNWs, in order to simplify the derivation, we assume that the concentration term ln(c_0/c_i) in Eq. (3) approximately corresponds to the variables term (kt) in Eq. (4), and the correction item ln(1/φ_i) can be roughly equated with the intercept (q) of the linear fitting equations. Equation (5) is thus easily obtained, and it is obviously a typical first order kinetics equation. Due to not ruling out the impact of mass transfer resistance during the derivation process, Eq. (5) is an apparent kinetic equation, and the apparent rate constant, the slope (k) of the linear fitting equations, is limited by two aspects: the reaction itself and mass transfer resistance.

$$\ln\frac{1}{\eta} = kt + \mathrm{q} \tag{4}$$

$$\ln\frac{c_0}{c_i} = -\ln\frac{c_i}{c_0} = kt \rightarrow c_i = c_0 \cdot \mathrm{e}^{-kt} \tag{5}$$

Oxygen plays a very crucial role in the oxidation process of ultrathin TeNWs. After bubbling oxygen into the reaction solution, it generally became saturated with oxygen and the MRR·η decreased from 1.0 to about 0.0. On increasing the flow rate of oxygen from 5 to 20 sccm, the downtrend of the

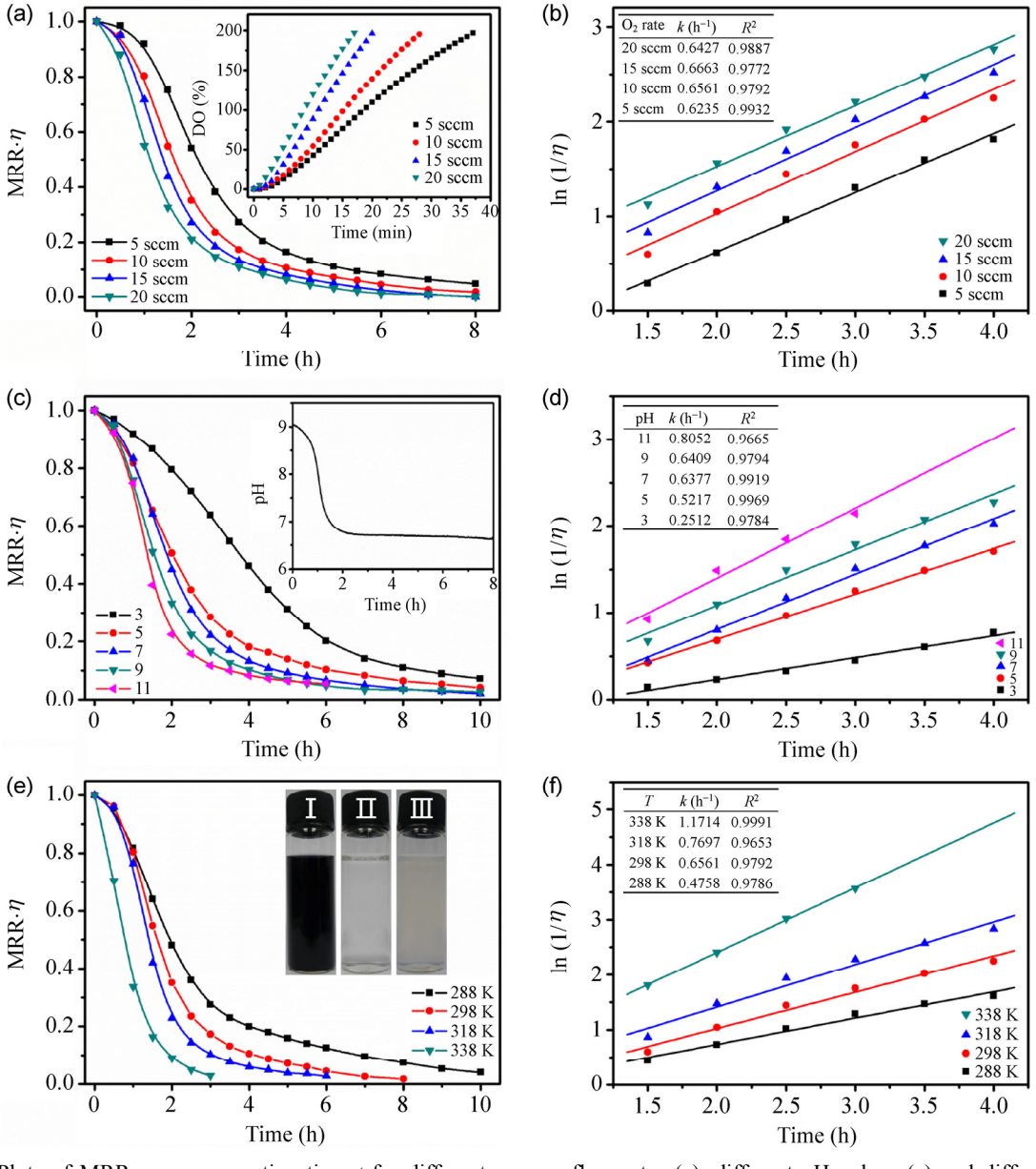

Figure 4 Plots of MRR·η versus reaction time t for different oxygen flow rates (a), different pH values (c) and different reaction temperatures (e). The linear fitting plots of the [ln(1/η)] versus reaction time t with different oxygen flow rates (b), at different pH values with an oxygen flow rate of 10 sccm (d), and at different reaction temperatures with an oxygen flow rate of 10 sccm (f). Inset in (a): plot of the dissolved oxygen versus the reaction time under different bubbling rates of oxygen. Inset in (c): plot of the pH value versus the reaction time at pH 9 at 298 K. Inset in (e): photographs of initial ultrathin TeNWs solution (I), completely oxidized ultrathin TeNWs solution (II), and after adding $AgNO_3$ to the completely oxidized ultrathin TeNWs solution (III). Insets in (b), (d) and (f): data for the corresponding linear fitting curves.

MRR·η was enhanced (Fig. 4(a)), while the apparent rate constants under different flow rates were approximately the same—only changing from 0.6235 to 0.6663 h^{-1}—because the reaction temperature was the same (298 K) (Fig. 4(b)). However, owing to the solid nature of ultrathin TeNWs, the oxygen flow rate is not the only factor that affects the oxidation rate, and the contact area between ultrathin TeNWs and oxygen also strongly influences the reaction rate. The contact area between ultrathin TeNWs and oxygen is closely linked with the dispersity of ultrathin TeNWs. In order to obtain a good dispersity of ultrathin TeNWs in solution, magnetic stirring for a long time and a suitable pH value were required.

The pH can influence the surface charge state of nanomaterials, and this is closely related to the extent of dispersion of nanomaterials. Meanwhile, hydroxyl ions or hydrogen ions can also act as a reactant and take part in the actual reaction. The increase in the value of [ln(1/η)] was much faster (Fig. 4(d)) when the solution was more alkaline, so high pH value obviously promotes the oxidation process. Indeed, when the pH value reached 13, ultrathin TeNWs would be completely oxidized within 1 h (Fig. S5(g), in the ESM). In contrast, more than 10 h was required at pH 1.0 (Fig. S5(a), in the ESM). There are two main reasons for this behavior: (i) ultrathin Te nanowires have a negative surface potential of about –16.45 mV. High pH values improve the dispersion of ultrathin TeNWs, which increases the contact area between the ultrathin TeNWs and oxygen by reducing the bundling and intertwining; (ii) hydroxyl ions can be involved in the oxidation process, since hydroxyl ions can react with ultrathin TeNWs (Eq. (6)) or with the oxidation product TeO_2 and promote the oxidation process (Eq. (7)). In order to distinguish between these two possibilities, ultrathin TeNWs were kept in solution at pH 9 with moderate magnetic stirring. The solution absorbance remained essentially unchanged on increasing the stirring time under the protection of nitrogen (Figs. 2(b) and 2(c)), showing that there is no reaction between ultrathin TeNWs and hydroxyl ions. But the absorbance dramatically decreased after bubbling oxygen through the solution (Fig. 2(a) and Figs. S4–S6, in the ESM) and the solution pH value quickly decreased from 9.0 to about 7.0 within two hours (as shown in the inset in Fig. 4(c)). Hence, hydroxyl ions are actually involved in the oxidation process by virtue of their reaction with oxidation products. The reaction between hydroxyl ions and the oxidation product TeO_2 can also be confirmed by the precipitation of silver tellurite(IV) (Ag_2TeO_3) (see the inset in Fig. 4(e)). Because the reaction between TeO_2 and hydroxyl ions reduced mass transfer resistance by consuming the oxidation products coated on the surfaces, the apparent rate constant showed a two- or three-fold increase at higher pH values (Fig. 4(d)), even although the oxidation experiments were performed at same reaction temperature (298 K).

$$3Te + 6OH^- = 2Te^{2-} + TeO_3^{2-} + 3H_2O \quad (6)$$

$$TeO_2 + 2OH^- = TeO_3^{2-} + H_2O \quad (7)$$

The oxidation process of ultrathin TeNWs is clearly a two-step process. Ultrathin TeNWs first react with oxygen to form TeO_2, and some of the TeO_2 falls of the surface into the solution to form small particles, with the remainder attached on the surface of ultrathin TeNWs. This blocks the contact between ultrathin TeNWs and oxygen, and is the main source of mass transfer resistance. Subsequently, the oxidation products TeO_2 reacts with hydroxyl ions to form TeO_3^{2-}, which can promote the oxidation of ultrathin TeNWs. As the oxidation proceeds, the surface of the ultrathin TeNWs becomes coated with oxidation products. When the quantity of the oxidation products accumulated to a sufficient extent, the mass transfer resistance can greatly limit the oxidation reaction. The increase in the conductivity of the reaction solution proves that the oxidation products TeO_2 was partly dissolved by water during oxidation (Fig. S8, in the ESM). Cheng et al. reported that the solubility of TeO_2 increases exponentially with increasing solution temperature [47]. Solution temperature also plays an important role in the reaction kinetics, so high reaction temperature favors both mass transfer and reaction kinetics. For a high temperature at 338 K, ultrathin TeNWs were completely oxidized within 3 h, but the reaction time was extended to 6 h at 318 K, to 8 h at 298 K and to 10 h at 288 K due to lower rates of oxidation and less dissolution of TeO_2 (Fig. 4(e)). At the same time, the apparent rate constant declined sharply from 1.1714 to 0.4758 h^{-1} (Fig. 4(f)). Generally, the reaction rate constant at least doubles when reaction temperature increases by 10 K, but the increase in this process is much smaller because of mass transfer resistance. The apparent activation energy of the reaction is defined as E_a in Eq. (8) based on the Arrhenius relation. In Eq. (8), R is the universal gas constant, T is the absolute temperature, B is the natural logarithm of the pre-exponential factor. By assuming the apparent activation energy to be independent of temperature from 288 to 338 K and fitting the data at different reaction temperatures, the apparent activation energy of this process was calculated to be about 13.53 kJ·mol^{-1}, indicating that the oxidation is a facile process (Fig. 5).

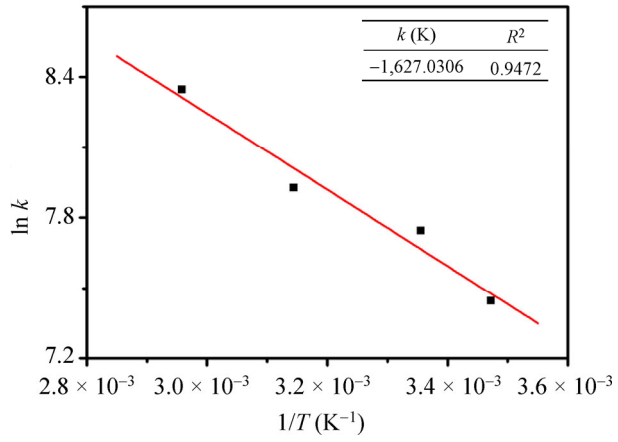

Figure 5 Linear fitting plot of the natural logarithm of the fitting apparent rate constant ln$k$ versus the reciprocal of the reaction temperature (1/T).

$$\ln k = -\frac{E_a}{RT} + B \quad (8)$$

3.5 Chemical transformation of ultrathin TeNWs during oxidation

The very low apparent activation energy (13.53 kJ·mol^{-1}) demonstrates that ultrathin TeNWs have a high reactivity. In our previous report, we showed the high reactivity of ultrathin TeNWs can provide fruitful grounds for exploring new nanoscale structural transformations as well as functionalities of the corresponding templated products. We investigate the reactivity of ultrathin TeNWs during oxidation from two perspectives. Firstly, as a physical template, oxidized ultrathin TeNWs were used to prepare Te@C nanocables through a template-directed hydrothermal carbonization process [38, 48]. Compared with highly uniform and long Te@C nanocables derived from normal ultrathin TeNWs (Fig. 6(a)), the Te@C nanocables obtained from oxidized TeNWs were short and bent (Fig. 6(b)), which is robust evidence for the fracture of ultrathin TeNWs during oxidation. Secondly, as a chemical template, oxidized ultrathin TeNWs were converted into Ag_2Te nanowires by reacting with silver nitrate in ethylene glycol. The products inherited the one-dimensional chain-dotted structure of ultrathin oxidized Te nanowires, which is difficult to achieve by a direct synthesis method, and had rougher surfaces than the normal Ag_2Te nanowires (Figs. 6(c) and 6(d)). The Jeong group [40] and our group [33] have previously shown that Ag_2Te nanowires can

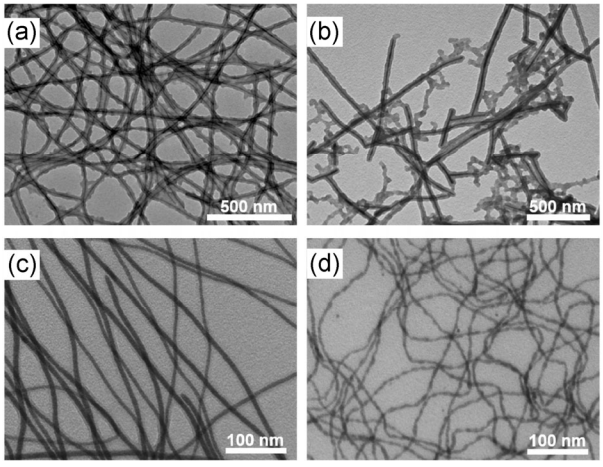

Figure 6 TEM images of the products templated from pristine TeNWs and TeNWs after oxidation. (a) Te@C nanocables synthesized from pristine ultrathin TeNWs, (b) Te@C nanocables synthesized from the TeNWs after oxidation for 2 h, (c) Ag_2Te nanowires synthesized from pristine TeNWs, (d) Ag_2Te nanowires synthesized from the TeNWs after oxidation for 1 h.

be transformed into other telluride nanowires (CdTe, ZnTe and PbTe) using cation-exchange reactions.

Here, we focus our study on the galvanic replacement reaction between TeNWs, as a chemical template, and H_2PtCl_6. It is interesting to note that the chemical transformation products showed a dramatic morphological-evolution from hollow nanotubular nanostructures to solid wire-like nanostructures (Figs. 7(a)–7(d) and Fig. S9(a), in the ESM), and even large particles (Figs. S9(b)–S9(d), in the ESM). A HRTEM image taken from an individual chemically transformed nanowire is shown in Fig. 7(e). The observed lattice spacings are 2.3 and 1.9 Å, which are consistent with the (111) plane and (200) plane of Pt, respectively. Figure 7(f) shows the XRD pattern of the chemical transformation products synthesized from the ultrathin TeNWs after oxidation for 1 h. All the diffraction peaks can be indexed to face-centered-cubic (f_{cc}) platinum, with a lattice constant of a = 3.9 Å (JCPDS No. 04-0802).

It is worthwhile to clearly understand why normal ultrathin TeNWs are transformed into a tubular nanostructure whereas oxidized ultrathin TeNWs are not. The Kirkendall effect, a classical phenomenon in metallurgy, has been used to illustrate the formation of hollow nanostructures [49–51]. On the basis of this mechanism, the different diffusion rates of two diffusion components result in a net outward flow, which leads

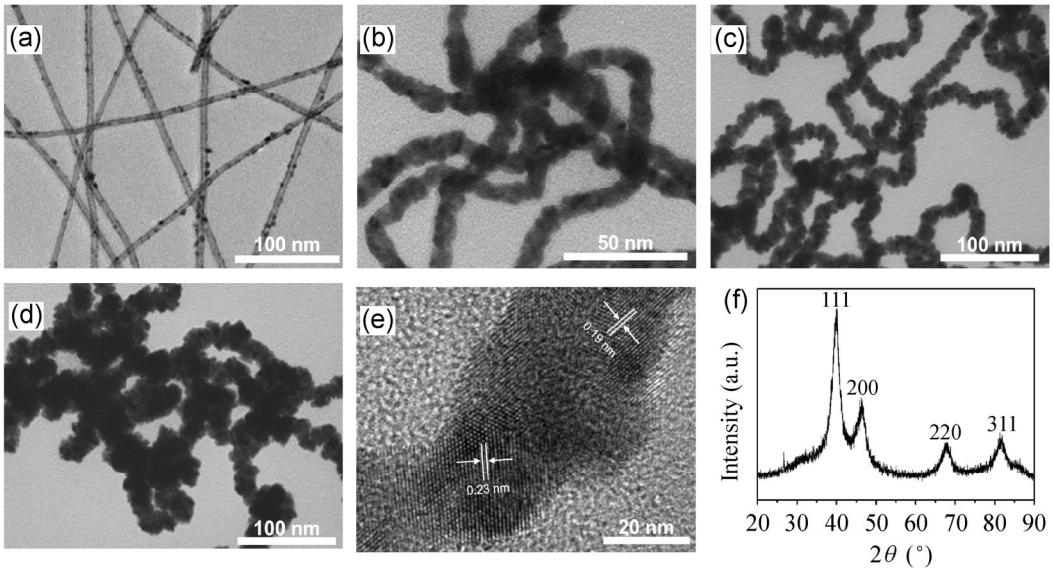

Figure 7 TEM images of the Pt nanostructures prepared by a chemical transformation process using the ultrathin TeNWs after oxidation for (a) 0, (b) 1, (c) 2, and (d) 3 h, as precursors. (e) HRTEM image of an individual solid wire-like Pt nanostructure obtained by chemical transformation using the ultrathin TeNWs after oxidation for 1 h. (f) XRD pattern of the sample prepared by a chemical transformation process using the ultrathin TeNWs after oxidation for 1 h as a precursor.

to the formation of hollow nanostructures. In the case of Pt nanotubes, the smooth surfaces of normal ultrathin TeNWs cause the galvanic replacement reaction to be limited in the radial direction of ultrathin TeNWs, therefore Te and Pt can continuously diffuse in opposite directions to form hollow tubular nanostructures (Fig. 7(a)). Because this reverse diffusion is slow at a low temperature, ultrathin TeNWs are not completely consumed. ICP–AES analyses indicated that the mass content of Te was maintained at about 20% in the chemical transformation products derived from normal ultrathin TeNWs, but decreased rapidly to 8% when ultrathin TeNWs were oxidized for only 0.5 h, and finally reached a constant value of about 3% (Fig. S10, in the ESM). In the case of oxidation, some ultrathin TeNWs were partially eroded or fractured, and the surface of all ultrathin TeNWs became fairly rough. The galvanic replacement reaction was not limited in the radial direction, but also occurred in the oxidation etching pits in other directions. The galvanic replacement reaction proceeded to a greater extent, and less Te was retained in these chemical transformation products. Furthermore, it was difficult to obtain sufficient net directional flow of matter to form a hollow nanostructure after the ultrathin TeNWs were oxidized. The morphology of the chemical transformation products evolved from hollow nanotubes (Fig. 7(a)) to nanowires with small pores (Fig. S9(a), in the ESM), solid nanowires (Figs. 7(b)–7(d)), and even large particles (Figs. S9(b)–S9(d), in the ESM), which were formed by an Ostwald ripening process.

3.6 Storage of ultrathin tellurium nanowires

The high reactivity of ultrathin TeNWs gives rise to a metastable nature, which can be easily degraded by oxidation during use. Astonishingly, ultrathin TeNWs can maintain their uniform morphology and high reactivity for more than six months in the original reaction solution, which includes PVP, $NH_3{\cdot}H_2O$, $N_2H_4{\cdot}H_2O$ and other by-product [36, 37]. It is very important to investigate the influence of PVP, $NH_3{\cdot}H_2O$, $N_2H_4{\cdot}H_2O$ on the stability of ultrathin TeNWs. Figure 8(a) shows digital photographs of ultrathin TeNWs stored under different conditions after different time intervals. On prolonging the storage time, all the samples showed a poor dispersity and settled to the bottom of sample bottle, and faded to colorless except for the sample stored in the presence of $N_2H_4{\cdot}H_2O$. The samples stored with mineral oil showed a lower oxidation rate, because mineral oil can, to some extent, prevent oxygen from dissolving in the solution. In addition, a low storage temperature is an excellent

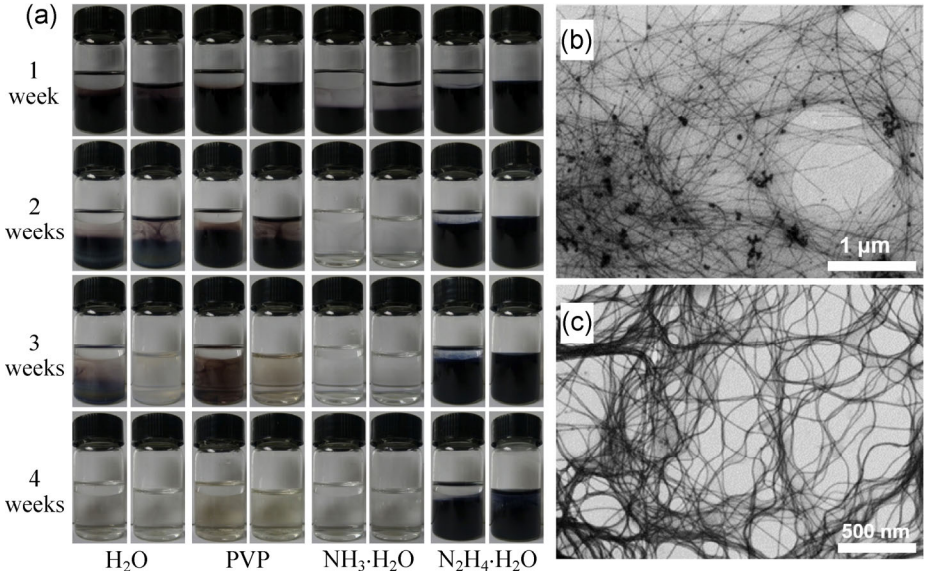

Figure 8 (a) Photographs of ultrathin TeNWs during storage with (left) and without (right) mineral oil for the sample with adding H_2O, PVP, $NH_3·H_2O$, $N_2H_4·H_2O$ at room temperature. TEM images of ultrathin TeNWs with adding $N_2H_4·H_2O$ after storage for 4 weeks without (b) and with (c) mineral oil.

way to inhibit oxidation of ultrathin TeNWs (Fig. S11, in the ESM).

Ultrathin TeNWs were generally oxidized in solution by the dissolved oxygen from air during storage. With the abscission of oxidation products, some PVP molecules were also shed from the surfaces of ultrathin TeNWs. Fewer PVP molecules coated on the surfaces of ultrathin TeNWs resulted in the poorer dispersity of ultrathin TeNWs in solution (Fig. 8(a)). Comparing the samples with and without PVP in the system, we found that adding the PVP capping agent did not give ultrathin TeNWs a good dispersity or protect them from oxidation. Adding $NH_3·H_2O$ to the storage solution produced an alkaline reaction medium, which promoted the oxidation process (Fig. 8(a)). Interestingly, when we added enough $NH_3·H_2O$ and a certain amount of PVP and $N_2H_4·H_2O$ to the completely oxidized storage solution, uniform ultrathin TeNWs with a length of 5-6 μm can be reproduced by hydrothermal reaction at 180 ℃ for 3 h (Fig. S12, in the ESM). This is not only a good way to reproduce ultrathin TeNWs after degradation, but also inspired us to synthesize ultrathin TeNWs using the cheaper and less toxic TeO_2.

When a certain amount of $N_2H_4·H_2O$ was added to the storage solution, the ultrathin TeNWs maintained a good stability for more than four weeks (Fig. 8(a)). Figures 8(b) and 8(c) show the TEM images of the sample with adding $N_2H_4·H_2O$ after storage for 4 weeks without or with mineral oil. The ultrathin TeNWs exhibited a uniform 1D nanowire morphology without any oxidation under the protection of $N_2H_4·H_2O$ and mineral oil after storing for 4 weeks. The standard electrode potentials of TeO_2/Te, O_2/H_2O and N_2/N_2H_4 are 0.593, 0.401 and –1.15 V. The difference between the redox potentials of the two half-cell reactions, ΔE, is –0.192 V for the reaction between O_2/H_2O and TeO_2/Te (Eq. (9)) and 1.551 V for the reaction between O_2/H_2O and N_2/N_2H_4 (Eq. (10)). Due to the reaction between O_2 and $N_2H_4·H_2O$ having a larger ΔE, oxygen can preferentially react with $N_2H_4·H_2O$. So $N_2H_4·H_2O$ can protect ultrathin TeNWs from oxidation by consuming oxygen. The reaction is thermodynamically possible only if ΔE is positive. The reaction between O_2 and tellurium has a negative potential, indicating the oxidation of tellurium is difficult. This is true for bulk tellurium, but ultrathin TeNWs are easily oxidized in water at room temperature. The main reason for this is that the ultrathin TeNWs have a large number of surface atoms which leave chemical bonds "dangling" outside the solid and this gives a higher reactivity than in the bulk [52].

$$Te + O_2 = TeO_2 \quad (9)$$

$$N_2H_4 + O_2 = N_2 + 2H_2O \quad (10)$$

We also investigated the storage of ultrathin TeNWs under other conditions at room temperature (Fig. 9). Comparing with the sample stored under ambient conditions, the sample under the protection of nitrogen still maintained a 1D nanowire morphology expect that some oxide particles were attached on the surfaces (Figs. 9(a) and 9(b)). The slight oxidation of ultrathin TeNWs could be attributed to the dissolved oxygen in water. Thus, an oxygen-free environment is beneficial for the storage of TeNWs. Ultrathin TeNWs exhibited a uniform 1D nanowire morphology without any oxidation under the protection of citric acid, ascorbic acid and $N_2H_4{\cdot}H_2O$ (Figs. 9(c)–9(e)). In addition, all the samples showed a good dispersity after storage for 10 days except the sample stored under ambient conditions and the sample stored in the presence of citric acid (Fig. 9(f)). Therefore, adding suitable reducing agents is an effective method to maintain uniform morphology and good dispersity for ultrathin TeNWs during storage. The degradation of ultrathin TeNWs during storage is a gas–solid oxidation reaction which involves liquid, gas and solid phases, so employing effective methods to prevent oxidation is the key to the storage of ultrathin TeNWs. Our results show that oxygen-free conditions and adding suitable reductants are effective ways to maintain the uniform morphology and high reactivity of ultrathin TeNWs during storage.

4 Conclusion

The stability of ultrathin TeNWs in aqueous solution has been investigated at different reaction temperatures, pH values and various oxygen flow rates from the viewpoint of reaction kinetics. Unlike traditional polyatomic organic molecules and metal complexes, due to the flexible features and size-dependent optical properties of ultrathin TeNWs, the absorbance of ultrathin TeNWs is related to several factors, namely concentration, dispersity, size and light scattering caused by ultrathin TeNWs and oxidation products. The oxidation of ultrathin TeNWs is a gas–solid reaction which involves liquid, gas and solid phases. The oxidation process can be divided into three stages, namely oxygen limiting, ultrathin TeNWs limiting and mass transfer resistance limiting stages. The apparent kinetics of this process accorded with a first order reaction kinetic model, and the corresponding apparent activation energy of this process was only 13.53 $kJ{\cdot}mol^{-1}$, indicating that ultrathin TeNWs are thermodynamically unstable.

However, the unstable nature of ultrathin TeNWs is actually an advantage because they can act as an

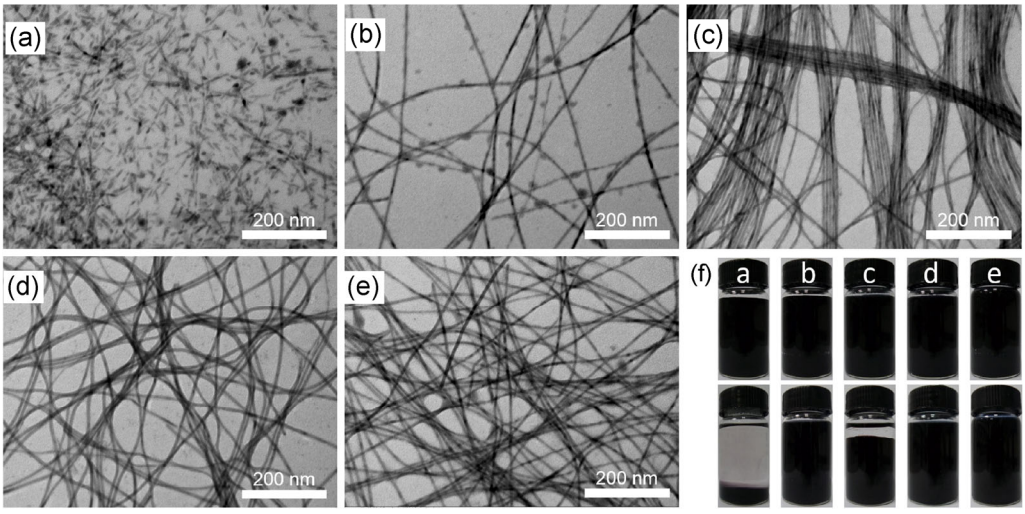

Figure 9 TEM images of ultrathin TeNWs after storage for 10 days (a) under ambient conditions, (b) in a vacuum desiccator, which was filled with nitrogen, (c) in the presence of citric acid, (d) in the presence of ascorbic acid, (e) in the presence of $N_2H_4{\cdot}H_2O$, (f) photographs of ultrathin TeNWs solution just after dispersion (top) and after storage for 10 days (bottom) under the different conditions.

excellent platform for the synthesis of unique one-dimensional functional nanomaterials with special structures and distinctive properties by using the intermediate nanostructures "captured" during the dynamic oxidation process under different conditions. This is difficult to achieve using existing direct synthesis methods. In addition, we found that oxygen-free conditions and adding suitable reductants are effective ways to prevent the oxidation of the freshly prepared ultrathin TeNWs and retain good stability during storage. The present work implies that knowing more about the stability and reactivity of nanomaterials is of great importance in designing functional nanomaterials based on chemical transformation process.

Acknowledgements

This work is supported by the National Basic Research Program of China (Grants 2010CB934700, 2013CB933900 and 2014CB931800), the National Natural Science Foundation of China (Grants 91022032, 91227103, 21061160492 and J1030412), and the Chinese Academy of Sciences (Grant KJZD-EW-M01-1) for financial support.

Electronic Supplementary Material: Supplementary material (details of characterization results and derivation process) is available in the online version of this article at http://dx.doi.org/10.1007/s12274-014-0586-9.

References

[1] Xia, Y. N.; Xiong, Y. J.; Lim, B.; Skrabalak, S. E. Shape-controlled synthesis of metal nanocrystals: Simple chemistry meets complex physics? *Angew. Chem. Int. Ed.* **2009**, *48*, 60–103.

[2] Yin, Y.; Alivisatos, A. P. Colloidal nanocrystal synthesis and the organic–inorganic interface. *Nature* **2005**, *437*, 664–670.

[3] Xia, Y. N.; Yang, P. D.; Sun, Y. G.; Wu, Y. Y.; Mayers, B.; Gates, B.; Yin, Y. D.; Kim, F.; Yan, Y. Q. One-dimensional nanostructures: Synthesis, characterization, and applications. *Adv. Mater.* **2003**, *15*, 353–389.

[4] Lim, B.; Jiang, M. J.; Yu, T.; Camargo, P. H. C.; Xia, Y. N. Nucleation and growth mechanisms for Pd–Pt bimetallic nanodendrites and their electrocatalytic properties. *Nano Res.* **2010**, *3*, 69–80.

[5] Mackenzie, J. D.; Bescher, E. P. Chemical routes in the synthesis of nanomaterials using the sol–gel process. *Acc. Chem. Res.* **2007**, *40*, 810–818.

[6] Ghosh Chaudhuri, R.; Paria, S. Core/shell nanoparticles: Classes, properties, synthesis mechanisms, characterization, and applications. *Chem. Rev.* **2012**, *112*, 2373–2433.

[7] Wang, D. S.; Xie, T.; Li, Y. D. Nanocrystals: Solution-based synthesis and applications as nanocatalysts. *Nano Res.* **2009**, *2*, 30–46.

[8] Walther, A.; Muller, A. H. E. Janus particles: Synthesis, self-assembly, physical properties, and applications. *Chem. Rev.* **2013**, *113*, 5194–5261.

[9] Xia, Y. S.; Tang, Z. Y. Monodisperse inorganic supraparticles: Formation mechanism, properties and applications. *Chem. Commun.* **2012**, *48*, 6320–6336.

[10] Wang, D. S.; Peng, Q.; Li, Y. D. Nanocrystalline intermetallics and alloys. *Nano Res.* **2010**, *3*, 574–580.

[11] Gong, J. X.; Li, G. D.; Tang, Z. Y. Self-assembly of noble metal nanocrystals: Fabrication, optical property, and application. *Nano Today* **2012**, *7*, 564–585.

[12] Pratt, A.; Lari, L.; Hovorka, O.; Shah, A.; Woffinden, C.; Tear, S. P.; Binns, C.; Kroger, R. Enhanced oxidation of nanoparticles through strain-mediated ionic transport. *Nat. Mater.* **2014**, *13*, 26–30.

[13] Andrievski, R. A. Review stability of nanostructured materials. *J. Mater. Sci.* **2003**, *38*, 1367–1375.

[14] Tang, Z. Y.; Kotov, N. A.; Giersig, M. Spontaneous organization of single CdTe nanoparticles into luminescent nanowires. *Science* **2002**, *297*, 237–240.

[15] Tang, Z. Y.; Wang, Y.; Shanbhag, S.; Giersig, M.; Kotov, N. A. Spontaneous transformation of CdTe nanoparticles into angled Te nanocrystals: From particles and rods to checkmarks, X-marks, and other unusual shapes. *J. Am. Chem. Soc.* **2006**, *128*, 6730–6736.

[16] Tang, Z. Y.; Wang, Y.; Sun, K.; Kotov, N. A. Spontaneous transformation of stabilizer-depleted binary semiconductor nanoparticles into selenium and tellurium nanowires. *Adv. Mater.* **2005**, *17*, 358–363.

[17] Moreels, I.; Fritzinger, B.; Martins, J. C.; Hens, Z. Surface chemistry of colloidal PbSe nanocrystals. *J. Am. Chem. Soc.* **2008**, *130*, 15081–15086.

[18] Xiong, Y. J. Morphological changes in Ag nanocrystals triggered by citrate photoreduction and governed by oxidative etching. *Chem. Commun.* **2011**, *47*, 1580–1582.

[19] Hung, L. I.; Tsung, C. K.; Huang, W. Y.; Yang, P. D.

Room-temperature formation of hollow Cu_2O nanoparticles. *Adv. Mater.* **2010**, *22*, 1910–1914.

[20] Mortimer, R. G. *Physical Chemistry*; Academic Press: London, 2008.

[21] Yu, W. W.; Qu, L. H.; Guo, W. Z.; Peng, X. G. Experimental determination of the extinction coefficient of CdTe, CdSe, and CdS nanocrystals. *Chem. Mater.* **2003**, *15*, 2854–2860.

[22] Peng, Z. A.; Peng, X. Nearly monodisperse and shape-controlled CdSe nanocrystals via alternative routes: Nucleation and growth. *J. Am. Chem. Soc.* **2002**, *124*, 3343–3353.

[23] Bunge, S. D.; Krueger, K. M.; Boyle, T. J.; Rodriguez, M. A.; Headley, T. J.; Colvin, V. L. Growth and morphology of cadmium chalcogenides: The synthesis of nanorods, tetrapods, and spheres from CdO and $Cd(O_2CCH_3)_2$. *J. Mater. Chem.* **2003**, *13*, 1705–1709.

[24] Xie, R. G.; Li, Z.; Peng, X. G. Nucleation kinetics vs. chemical kinetics in the initial formation of semiconductor nanocrystals. *J. Am. Chem. Soc.* **2009**, *131*, 15457–15466.

[25] Peng, X. G. An essay on synthetic chemistry of colloidal nanocrystals. *Nano Res.* **2009**, *2*, 425–447.

[26] Qian, H. S.; Yu, S. H.; Gong, J. Y.; Luo, L. B.; Fei, L. F. High-quality luminescent tellurium nanowires of several nanometers in diameter and high aspect ratio synthesized by a poly(vinyl pyrrolidone)-assisted hydrothermal process. *Langmuir* **2006**, *22*, 3830–3835.

[27] Liang, H. W.; Liu, J. W.; Qian, H. S.; Yu, S. H. Multiplex templating process in one-dimensional nanoscale: Controllable synthesis, macroscopic assemblies, and applications. *Acc. Chem. Res.* **2013**, *46*, 1450–1461.

[28] Liang, H. W.; Cao, X.; Zhou, F.; Cui, C. H.; Zhang, W. J.; Yu, S. H. A free-standing Pt-nanowire membrane as a highly stable electrocatalyst for the oxygen reduction reaction. *Adv. Mater.* **2011**, *23*, 1467–1471.

[29] Liang, H. W.; Liu, S.; Yu, S. H. Controlled synthesis of one-dimensional inorganic nanostructures using pre-existing one-dimensional nanostructures as templates. *Adv. Mater.* **2010**, *22*, 3925–3937.

[30] Li, H. H.; Zhao, S.; Gong, M.; Cui, C. H.; He, D.; Liang, H. W.; Wu, L.; Yu, S. H. Ultrathin PtPdTe nanowires as superior catalysts for methanol electrooxidation. *Angew. Chem. Int. Ed.* **2013**, *52*, 7472–7476.

[31] Chen, L. F.; Zhang, X. D.; Liang, H. W.; Kong, M. G.; Guan, Q. F.; Chen, P.; Wu, Z. Y.; Yu, S. H. Synthesis of nitrogen-doped porous carbon nanofibers as an efficient electrode material for supercapacitors. *ACS Nano* **2012**, *6*, 7092–7102.

[32] Wang, K.; Liang, H. W.; Yao, W. T.; Yu, S. H. Templating synthesis of uniform Bi_2Te_3 nanowires with high aspect ratio in triethylene glycol (TEG) and their thermoelectric performance. *J. Mater. Chem.* **2011**, *21*, 15057–15062.

[33] Liu, J. W.; Xu, J.; Liang, H. W.; Wang, K.; Yu, S. H. Macroscale ordered ultrathin telluride nanowire films, and tellurium/telluride hetero-nanowire films. *Angew. Chem. Int. Ed.* **2012**, *51*, 7420–7425.

[34] Wu, Z. Y.; Li, C.; Liang, H. W.; Chen, J. F.; Yu, S. H. Ultralight, flexible, and fire-resistant carbon nanofiber aerogels from bacterial cellulose. *Angew. Chem. Int. Ed.* **2013**, *52*, 2925–2929.

[35] Liang, H. W.; Cao, X.; Zhang, W. J.; Lin, H. T.; Zhou, F.; Chen, L. F.; Yu, S. H. Robust and highly efficient free-standing carbonaceous nanofiber membranes for water purification. *Adv. Funct. Mater.* **2011**, *21*, 3851–3858.

[36] Lan, W. J.; Yu, S. H.; Qian, H. S.; Wan, Y. Dispersibility, stabilization, and chemical stability of ultrathin tellurium nanowires in acetone: Morphology change, crystallization, and transformation into TeO_2 in different solvents. *Langmuir* **2007**, *23*, 3409–3417.

[37] Liu, J. W.; Chen, F.; Zhang, M.; Qi, H.; Zhang, C. L.; Yu, S. H. Rapid microwave-assisted synthesis of uniform ultralong Te nanowires, optical property, and chemical stability. *Langmuir* **2010**, *26*, 11372–11377.

[38] Liang, H. W.; Zhang, W. J.; Ma, Y. N.; Cao, X.; Guan, Q. F.; Xu, W. P.; Yu, S. H. Highly active carbonaceous nanofibers: A versatile scaffold for constructing multifunctional free-standing membranes. *ACS Nano* **2011**, *5*, 8148–8161.

[39] Qian, H. S.; Yu, S. H.; Luo, L. B.; Gong, J. Y.; Fei, L. F.; Liu, X. M. Synthesis of uniform Te@carbon-rich composite nanocables with photoluminescence properties and carbonaceous nanofibers by the hydrothermal carbonization of glucose. *Chem. Mater.* **2006**, *18*, 2102–2108.

[40] Moon, G. D.; Ko, S.; Xia, Y.; Jeong, U. Chemical transformations in ultrathin chalcogenide nanowires. *ACS Nano* **2010**, *4*, 2307–2319.

[41] Lin, Z. H.; Yang, Z. S.; Chang, H. T. Preparation of fluorescent tellurium nanowires at room temperature. *Cryst. Growth. Des.* **2008**, *8*, 351–357.

[42] Isomäki, H. M.; von Boehm, J. Optical absorption of tellurium. *Phys. Scr.* **1981**, *25*, 801–803.

[43] Gautam, U. K.; Rao, C. N. R. Controlled synthesis of crystalline tellurium nanorods, nanowires, nanobelts and related structures by a self-seeding solution process. *J. Mater. Chem.* **2004**, *14*, 2530–2535.

[44] Bohren, C. F.; Huffman, D. R. *Absorption and Scattering of Light by Small Particles*; Wiley Interscience: New York, 1983.

[45] Cademartiri, L.; Montanari, E.; Calestani, G.; Migliori, A.; Guagliardi, A.; Ozin, G. A. Size-dependent extinction coefficients of PbS quantum dots. *J. Am. Chem. Soc.* **2006**, *128*, 10337–10346.

[46] Darbha, G. K.; Singh, A. K.; Rai, U. S.; Yu, E.; Yu, H. T.; Ray, P. C. Selective detection of mercury(II) ion using nonlinear optical properties of gold nanoparticles. *J. Am. Chem. Soc.* **2008**, *130*, 8038–8043.

[47] Cheng, K. L. Analysis of lead telluride with an accuracy to better than 0.1%. *Anal. Chem.* **1961**, *33*, 761–764.

[48] Liang, H. W.; Guan, Q. F.; Chen, L. F.; Zhu, Z.; Zhang, W. J.; Yu, S. H. Macroscopic-scale template synthesis of robust carbonaceous nanofiber hydrogels and aerogels and their applications. *Angew. Chem. Int. Ed.* **2012**, *51*, 5101–5105.

[49] Yin, Y. D.; Rioux, R. M.; Erdonmez, C. K.; Hughes, S.; Somorjai, G. A.; Alivisatos, A. P. Formation of hollow nanocrystals through the nanoscale Kirkendall effect. *Science* **2004**, *304*, 711–714.

[50] Wang, W. S.; Dahl, M.; Yin, Y. D. Hollow nanocrystals through the nanoscale Kirkendall effect. *Chem. Mater.* **2013**, *25*, 1179–1189.

[51] Fan, H. J.; Knez, M.; Scholz, R.; Nielsch, K.; Pippel, E.; Hesse, D.; Zacharias, M.; Gosele, U. Monocrystalline spinel nanotube fabrication based on the Kirkendall effect. *Nat. Mater.* **2006**, *5*, 627–631.

[52] Nalwa, H. S. *Handbook of Nanostructured Materials and Nanotechnology*; Academic Press: London, 2000.